Kuwait J.Sci., Vol.50, No.(3A),July.2023,pp(1-19)

Synthesis of ternary nanocomposites of GO–MnO_2@Tau and GO-MnO_2@CA for efficient removal of dyes

Iram Bibi[1], Khalid Raza[1], Wajid Rehman[1,*], Siddiqa Begum[1], Magda H. Abdellatif [2], Saz Muhammad[2], Syed. Waqar H. Shah[1], Luqman A. Shah[3], Saira Bibi[1], Wajhia Khan[4]

[1]*Dept. of Chemistry, Hazara University 21120, Mansehra, KP, Pakistan*
[2]*Dept. of Chemistry, College of Sciences, Taif University, P. O Box 11099 Taif 21944, Saudi Arabia.*
[3]*Faculty of Basic Sciences, Kohsar University Murree, 47150, Rawalpindi, Punjab, Pakistan.*
[3]*National Centre of Excellence in Physical Chemistry, Peshawar University, Peshawar, KP, Pakistan*
[4]*Dept. of biotechnology COMSATS University Islamabad, Abbottabad campus, Pakistan*

*****Corresponding author: sono_waj@yahoo.com*

Abstract

Here, we report the facile route for the synthesis of graphene oxide–functionalized manganese dioxide (GO–MnO_2@Tau (GMT) and GO-MnO_2@CA) (GMC) nanohybrids and their use as adsorbents for removal of selected dyes from industrial effluents. These nanohybrids were also tested for antibacterial activity in wastewater. Manganese dioxide nanoparticles were synthesized by redox reaction between potassium permanganate ($KMnO_4$) and manganese acetate ($Mn(CH_3COO)_2.4H_2O$) and functionalized with taurine ($H_3N^+CH_2CH_2SO_3^-$) and caproic acid ($CH_3(CH_2)_8COOH$) to produce MnO_2@Tau and MnO_2@CA. These functionalized-MnO_2 were then exploited as reinforcement in graphene oxide (GO) to fabricate nanohybrids. The nanohybrids were characterized for their morphology, structure, crystallinity and thermal behavior by scanning electron microscopy (SEM), X-ray diffraction (XRD), Fourier transform infra-red (FTIR) spectroscopy, UV-Visible spectroscopy and thermogravimetric analysis (TGA). The results were reproducible with negligible variation in physical properties among different batches. They were investigated for adsorptive removal of methylene blue and malachite green and effect of temperature and quantity of adsorbent were studied. The adsorption of both dyes followed *pseudo* second order kinetics. The addition of MnO_2@tau and MnO_2@CA as nanofillers within GO has led to decrease in its crystallinity. This may be attributed to the dispersion of MnO_2@tau and MnO_2@CA within layers of GO which causes breakage of regular stacks of GO. The antibacterial activity of GO-MnO2@Tau and GO-MnO2@CA nanohybrids were tested against two bacterial strains (Gram-negative *E. coli*, and the Gram-positive *S. aureus*) and the results revealed efficient inhibition of these pathogens.

Keywords: Bacterial strains; graphene oxide–functionalized manganese dioxide; manganese dioxide nanoparticles; nanohybrids; ternary.

1. Introduction

Graphene has shown diverse applications in the field of biomedicine, oncotherapy, drug delivery and imaging due to its high surface area, easy functionalization, extraordinary optical and electrical properties and superior mechanical strength (Wang, H., *et al.,* 2019). Graphene oxide (GO) is a derivative of graphene that has two-dimensional hydrophobic structure, but its basal plane contains epoxide and hydroxyl groups, whereas edges comprise carboxyl groups. Previous studies showed that peptides possessed strong affinity for graphene oxide (GO) due to hydrophobic and electrostatic interactions (Pattnaik, S., *et al.,* 2016; Zhang, Y., *et al.,* 2012).

Manganese dioxide (MnO_2) is amongst the most attractive transition metal oxides with high activity and low cost. Hence, it is often harnessed in catalysis, energy storage devices and formation of ion-selective molecular sieves. Owing to catalytic activity, high surface area and high adsorption capability of MnO_2 acts as a potential destructive adsorbent in water treatment (Wang, N., *et al.,* 2016). Hierarchical hollow MnO_2 has shown an efficient ability to remove organic dyes and toxic metal ions, but its separation from treated water is a major drawback (Fei, J. B*., et al.,* 2008). Monolithic MnO_2 having porous structure is an ideal candidate for water treatment, but its use is limited by agglomeration of its nanoparticles. Moreover, its intrinsic fragility that makes it crack or collapse under small stress or deformation limits it utility (Lei, Z., *et al.,* 2012). To address this problem MnO_2 nanocomposites have been synthesized. (Qu, J., *et al.,* 2014**)** synthesized nanocomposites of MnO_2-GO hybrid and reported the ultrafast oxidative decomposition of methylene blue dye using them. (Wang, N., *et al.,* 2016) synthesized monolithic polyurethane, reduced graphene oxide and manganese dioxide (PU@RGO@MnO_2) hybrid sponges for efficient removal of methylene blue. The PU sponge provides the monolithic adsorbent enough flexibility, while RGO prevents agglomeration. (Hoseinpour,V., *et al.,* 2018) synthesized triple nanocomposites (TNC) of ZnO-MnO_2-Cu_2O (ZMC). TNC show significant antimicrobial activity of E.coli and Staphyloccus aureus. (Kumar, R.R., *et al.,* 2022) synthesized MnO_2/GO nanocomposites through simple chemical route. They studied the electrical properties with different mass ratio of the matrix and filler. These nanocomposites were coated on SS by electrodeposition method which led to the finding that these nanocomposites possess enhanced conduction properties. The investigation on electrical properties led to the finding that the composite can be used as supercapacitor having far better potential than conventional capacitors and other electronic devices. (Balasubramanian, N., *et al.,* 2022) synthesized MnO2 cube /r-GO nanocomposites by simple hydrothermal method and studied their electrochemical properties by using nanocomposites as anode and rGo as cathode. The investigation revealed that this asymmetric supercapacitor possesses high specific capacitance of 92.49Fg-1 at 1 A g^{-1} owing to 1.5860 Wkg^{-1} high power density and 17.7555 Wh kg^{-1} high energy density at 8 A g-1. This nanocomposites has considered as excellent material for energy storage.

Herein, this research study is designed to graft the MnO_2 with different chemicals moieties i.e. taurine and caproic acid then exploited them as nanofillers within GO matrix for the fabrication of nanohybrids of MnO_2@Tau/GO and MnO_2@CA/GO. These nanohybrids were exploited as adsorbent for the removal of selected organic dyes i.e. MB and MG from water along with

investigation as antibacterial agents in aqueous solutions on Gram-negative *E. coli*, and the Gram-positive *S. aureus*

2. Experimental

2.1 Synthesis of MnO_2 Nanoparticles

MnO_2 nanoparticles were synthesized by redox reaction between potassium permanganate ($KMnO_4$) and manganese acetate ($Mn(CH_3COO)_2.4H_2O$). Initially, aqueous solutions of $KMnO_4$ (0.1M) and $Mn(CH_3COO)_2.4H_2O$ (0.15 M) were separately prepared in deionized water. Then both solutions were mixed and stirred for ample of timer to ensure homogeneity and completion of reaction. The nanoparticles thus obtained were washed with H_2O and ethanol, filtered and oven-dried at 85ºC for 12h (Qu, J., *et al.,* 2014).

2.2 Synthesis of Graphene Oxide (GO)

GO was prepared from graphite using the Hummers method (Wei, C., *et al.,* 2012). Initially, graphite powder (2g) and $NaNO_3$ (2g) were mixed in a volumetric flask and kept in the ice bath (0–5ºC) with continuous stirring for 4h. This was followed by gradual addition of $KMnO_4$ (12g). The mixture was diluted by adding 184 ml of distilled water slowly and stirred for further 2h at 35ºC. The resulting reaction mixture was refluxed at 98ºC for 10 to 15 minutes. After reflux, the solution was kept at 30°C for 10 minutes, after which brown coloration was developed. The stirring was continued for another 2 h at 25ºC, after which 40 ml of hydrogen peroxide (H_2O_2) were added. At this stage the color of solution changed from brown to bright yellow. The resulting mixture was diluted with 200 ml water and allowed to stand for 3–4h. The resulting GO particles was kept for 3-4 hours to settle down. Finally, the GO particles were collected via centrifugation, washed with 10% HCl solution as well as distilled water and oven dried 70ºC (Paulchamy, B., *et al.,* 2015).

2.3 General Procedure for Synthesis of MnO_2@Tau and MnO_2@CA)

For the synthesis of MnO_2@Tau (or MnO_2@CA), 1.2g of MnO_2 were dissolved in 40 ml of distilled water and stirred for 1h. To the resulting black colored solution, an aqueous solution containing 0.4g Tau (or CA) in 40 ml of distilled water was added. The temperature was then raised to 55 to 60 ºC and stirring was continued at this temperature for 4 hours. The final product was obtained by centrifugation and then oven-dried for 8 hours.

2.4 General Procedure for Synthesis of Nanocomposites (GO-MnO_2@CA or GO-MnO_2@Tau)

Nanocomposites based on G0-MnO with either taurine or caproic acid were synthesized by using simple strategy. GO (0.2g) was dispersed in 50 ml distilled water and sonicated for 2 h in an ice bath followed by 1h of stirring. Separately, 0.2g of MnO_2@CA or MnO_2@Tau were dissolved in

50 mL of distilled water through stirring (1.5h). The two solutions were mixed and stirred for 2h, at 55-62ºC. The product was obtained in the form of black precipitate, which was collected through centrifugation and oven-dried at 75ºC for 8-10 hours.

2.5 Characterization of Samples

Each sample was characterized by using different techniques. The electronic absorption patterns were obtained through double beam UV–Vis 1601 Shimadzu spectrophotometer. The surface functionalization of samples was investigated by PLATINUM-ATR ALPHA (BRUKER) FTIR in the range of 4000–500 cm^{-1}.To study the crystalline nature of samples X-ray diffraction technique with an X-ray Diffractometer D8 Advanced Davinci by Bruker having Cu kα radiation (1.54Å) source, operated at 40 KV voltage and 30 mA currents was used. Morphological studies were carried out with the help of scanning electron microscopy (SEM, MIRA3 TESCAN) operating at 10 KV. Thermal analysis was carried out with the help of TGA from Mettler Toledo Switzerland (Model: TGA/DSC1). During all measurements heating rate was kept constant (10°C/min) in a temperature range of 25 to 1000°C under nitrogen flow of 50 mL/min.

3. Results and Discussion

3.1 UV-visible Spectroscopic Analysis

UV-Visible absorption spectra of GO shown in Figure. 1. (a) represent two broad absorptions in the ultraviolet region i.e., 209 nm and 280 nm. These peaks correspond to π–π* transition of the C=C bond and n–π* transition of the C=O groups, respectively (Çiplak, Z., *et al.,* 2015; Baruah, U., et al., 2018).

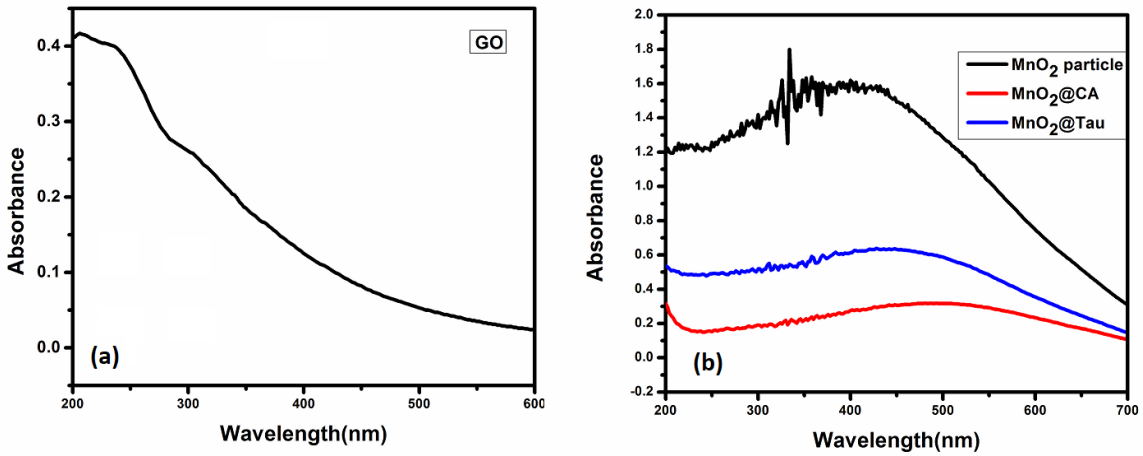

Fig. 1. (a) UV-Visible spectra of GO (b) UV-Visible spectra of MnO_2, MnO_2CA(CA) and MnO_2@Tau(TA)

The electronic spectra of MnO_2 nanoparticles, MnO_2@CA (designated as CA) and MnO_2@Tau (represented as TA) are gathered in Figure. 1. (b) The λ_{max} at 335nm is ascribed to d–d transitions of Mn ions in MnO_2 nanoparticles (Gupta, V. K., *et al.,* 2017; Hoseinpour, V., *et al.,* 2018). The broadbands at 450-550 nm and 410-490 nm in functionalized NPs are due to electronic transitions of taurine and caproic acid grafts (Yugambica, S.; Yu, T., *et al.,* 2017).

The UV-Visible spectra of nanohybrids are shown in the Figure 2**.** In these spectra the emergence of peaks at 250 nm in case of GO-MnO_2@CA (GMC) and 240 nm in GO-MnO_2@Tau (GMT) could be attributed to the interaction of nanofillers with GO matrix. The UV results are reproducible within ± 0.3 nm.

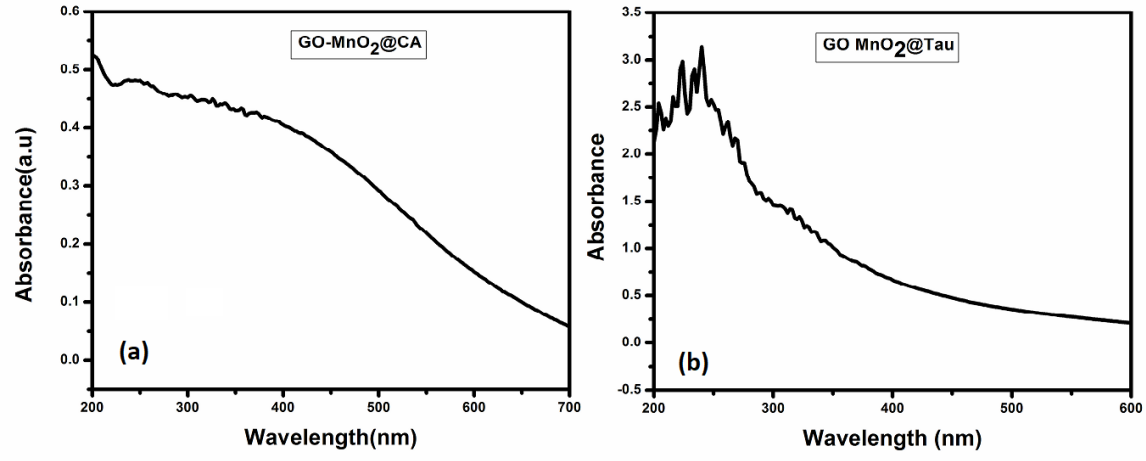

Fig. 2. UV-Visible of GO- MnO_2@CA and GO-MnO_2@Tau.

3.2 XRD Analysis

To investigate the crystallinity of MnO_2, MnO_2@Tau and GO and its nanohybrids with MnO_2@Tau and MnO_2@CA the XRD studies were carried out in the range of 2θ from 10-80° The diffraction pattern of the pure MnO_2 gives peak at 2θ=12.7°,27.9°,37.5°,49.2°,58.9°,and 65.3° from reflection planes (110), (310), (211), (411), (521) and (002) respectively are shown in Figure 3. (a) (Wang, J. W., *et al.,* 2015; Yang, W., *et al.,* 2017; Gund, G. S., *et al.,* 2015). In pure state, MnO_2 exists in α-phase and the change in intensity of characteristic peaks of MnO_2 is observed in MnO_2@CA and MnO_2@Tau. The intensity of peak at 2θ value of 37.5° that corresponds to (211) reflection decreases in both MnO_2@Tau and MnO_2@CA. The intensity of peak specified for α-MnO_2 are observed to decrease by grafting with CA and TA at its surface are given in Figure 3**.** (b). Similarly, the intensity of the peaks corresponding to (12.7°) and (65.3°) from (110) and (002) are also observed to decrease sharply in MnO_2@ CA and almost diminish in MnO_2@Tau (Hu, Z., *et al.,* 2015).

The pure GO has given a diffraction plane (002) at 11.2° correspond to the distance (0.34 nm) between graphene layers. The peak at 42.26° gives a diffraction plane (100) which is indicating the short order in stacked graphene layers as shown in Figure 3. (b) (Wu, H., *et al.,* 2014; Rafi, M., *et al.,* 2018; Stobinski, L., *et al.,* 2014). It can be seen that by the treatment of

functionalized GO (MnO_2@Tau and MnO_2@CA) has led to the change in the crystallinity of GO as shown in Figure 3. (b). The peak of pure GO is weekend or almost disappear which can be seen from XRD pattern of GO-MnO_2@tau and GO-MnO_2@CA nanohybrids. This may be attributed the interaction of nanofillers with GO has resulted in lowering the intensity of peak of GO matrix thus led to change in its crystallinity. In case of GO-MnO_2@Tau the decrease in the intensity of peak at 11.2° for (002) reflection is pronounced while it was observed to be completely vanished in GO-MnO_2@CA. The intensity of the another peak corresponding to (100) reflection plane of the of pure GO at (42.26°) has been observed to be reduced in case of GO-MnO_2@Tau and disappeared GO-MnO_2@CA.The decrease in the crystallinity of the GO upon the addition of MnO_2@tau and MnO_2@CA as nanofillers is assumed to be accommodation between the layers of GO thus led to breakage of regular stacks of GO (Singu, B. S., *et al.,* 2017). After functionalization of MnO2 nanoparticles by either CA or TAU, the crystallinity is affected negligibly. However, it is markedly reduced in nanohybrids with GO. This is likely to have a bearing on properties like adsorption capacity and light harnessing capability.

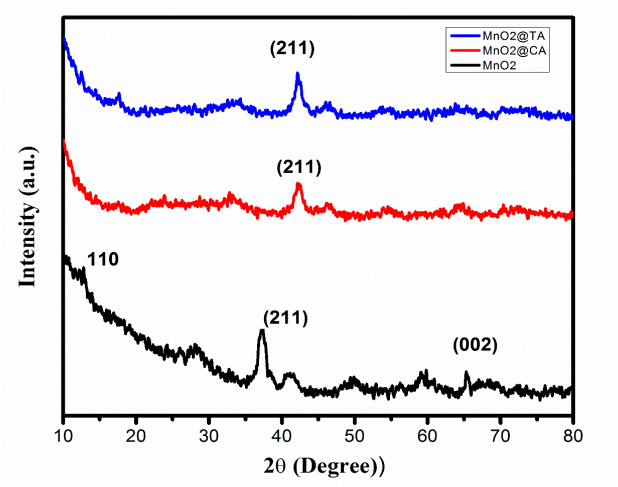

Fig. 3. (a) XRD spectrum of MnO_2 and MnO_2@tau &MnO_2@CA

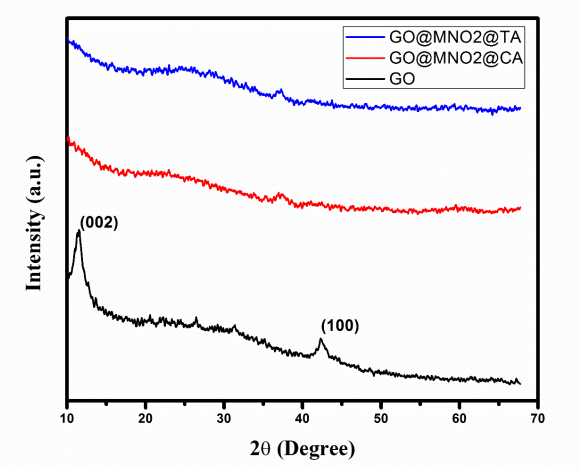

Fig. 3. (b) XRD Spectra of GO and GO-MnO_2@CA & GO-MnO_2@Tau.

3.3 Fourier Transform Infrared Spectroscopic Analysis

FTIR spectra were recorded in ATR mode in the range of 4000-500cm^{-1} to investigate the structural features of MnO_2, MnO_2@CA and MnO_2@Tau. GO and nanohybrids of GO-MnO_2@CA and MnO_2@Tau (Fig 4). The FTIR spectrum of MnO_2 nanoparticle is represented in Figure 4. (a). The transmittance peaks at 719.71, 414.51 and a peak around 540 corresponds to Mn-O vibrational band of α-MnO_2 **(**Walton, I. M., *et al.,* 2016). The FTIR of MnO_2@CA hybrid shared identical peaks with MnO_2, but some new peaks have appeared at 1739.61cm^{-1}, 1216.86cm^{-1} and 1629.08cm^{-1}. They are attributed to C=O, C–O stretching vibrations and C=C stretching of alkene respectively as shown in Figure 4. (a). These vibrations clearly indicate that MnO_2 particles were anchored to the caproic acid.

FTIR of MnO_2@Tau FTIR was carried to study the structural changes in MnO_2 upon grafting with taurine is represented in the Figure. 4. (a). There has been observed the characteristics bands for both MnO_2 and taurine. The bands appeared at 1737.97 cm^{-1},1216.67 and 1366.67 cm^{-1} are associated with the C=O stretching vibration, sulfonic acid group –SO_3H and sulfonate group (-SO_3^-) respectively. The transmittance peak at 1631.60cm^{-1} is related to the C=C cm^{-1} (stretching vibration) of alkenes (Kumar, N., *et al.,* 2014; Elemike, E. E., *et al.,* 2016) and the broad peaks at 3256.69cm^{-1} corresponds to stretching of OH and a small peak around 2930cm^{-1} to C-H stretching vibration. The peaks of the MnO_2 appeared below 800cm^{-1},719.7cm^{-1}, 422.47 cm^{-1}. The appearance of characterized bands belonging to Tau is an indication of successful grafting at the surface of MnO_2.

FTIR spectrum of the GO corresponds to bands for various oxygen containing functional groups are shown in Figure 4. (a). The peak at 3028.28cm^{-1} and 3412cm^{-1} shows the OH stretching vibration of absorbed moisture on the sample and the peaks at 1738.37cm^{-1},1047.86cm^{-1} are related to the stretching vibration of C=O (carboxylic acid) and C─O (epoxide group). The bands at 1617.34 cm^{-1} and 1366.09 cm^{-1} correspond the stretching vibration of C=C of alkene and C-OH of carboxyl (Ossonon, B. D., *et al.,* 2017; Beshir, L., M. 2018; Sharma, N., *et al.,* 2017). A very weak band at 2970.41 cm^{-1} is related to symmetric and asymmetric stretching vibration of C–H bond and C–O stretching of epoxy groups (1216.16cm^{-1}) respectively.

The FTIR spectra of GO- MnO_2@CA nanohybrids is given in Figure. 4. (b). The characteristics peaks of both GO and MnO_2@CA can be seen within the spectrum. The characteristics bands of GO can be observed to be appeared with slight shifting at 3026.42cm^{-1}, 2970.33cm^{-1} and 1038.84cm^{-1} along with the band of Mn-O and Mn-O-Mn vibrations within GO-MnO_2@CA nanohybrids. The combination of peaks of GO and MnO_2@CA in GO-MnO_2@CA has revealed the strong interaction between filler and matrix within GO–MnO_2@CA nanohybrids. FTIR spectra of GO-MnO_2@Tau nanohybrids were recorded in ATR mode from 4000–500cm^{-1} as shown in Figure 4. (b). As compared to neat GO there has been observed the characteristics peaks of MnO_2@Tau nanofiller and GO matrix within nanohybrids. The characteristics peaks of GO at 3028.26cm^{-1} and 1047.47cm^{-1} were observed to shift to 3016.42cm^{-1} and 1052.07cm^{-1} in its hybrid with MnO_2@Tau. The band at 1617.34 cm^{-1} of GO was disappeared in GO-MnO_2@Tau and shows a new peak at 1577.09 cm^{-1} due to the stretching vibration of N-H. Additionally, the

band of Mn-O and Mn-O-Mn vibration was observed, in the case of GO-MnO_2@Tau. The interaction between MnO_2@ Tau and GO has resulted in the shift of characteristics peak of the matrix. This shifting in peaks may be attributed to the strong interaction between filler and matrix within GO-MnO_2@Tau. The FTIR results are reproducible within ±2 cm^{-1}.

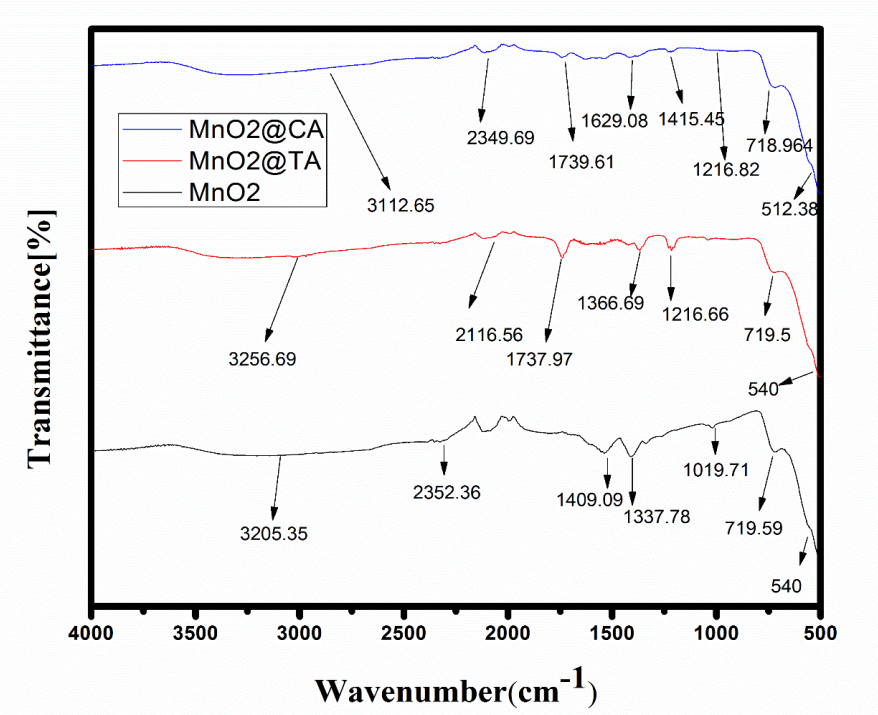

Fig. 4. (a). FTIR spectrum of MnO_2, MnO_2CA MnO_2@Tau.

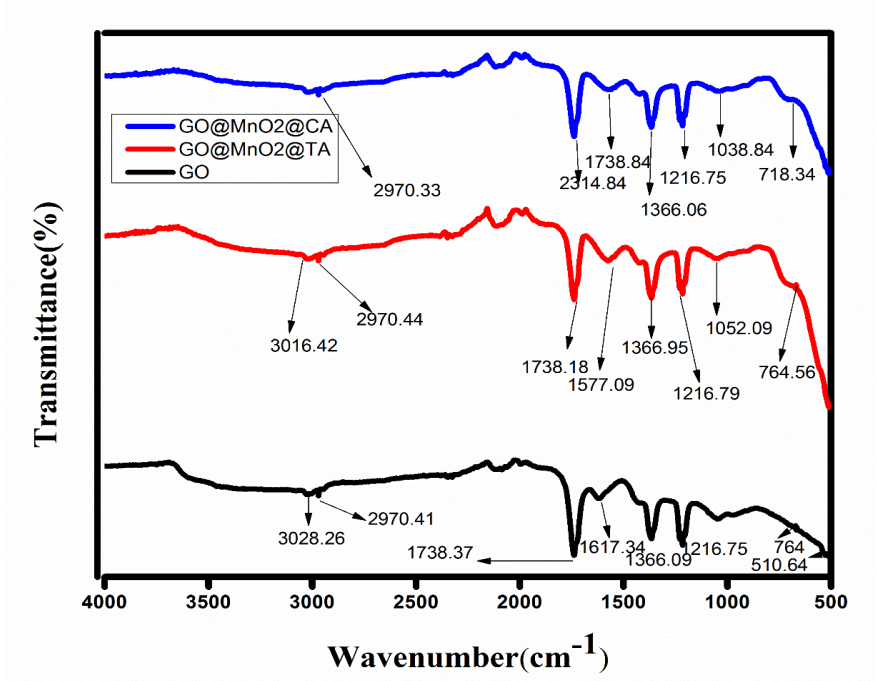

Fig. 4. (b). FTIR spectrum of GO-MnO_2@Tau

3.4 SEM

SEM images were taken at various magnification ranging from 1µm to 0.1 µm to study the morphology of synthesized nanohybrids of GO with MnO_2@CA shown in Figure. 5. (a), (b). In SEM micrographs of the GO-MnO_2@CA the MnO_2@CA particles are seen to be homogeneously dispersed in GO sheets and GO sheets are exfoliated and decorated randomly within MnO_2@CA. In the SEM micrographs of GO-MnO_2@Tau shown in Figure 6, it can be seen that MnO_2@Tau is distributed uniformly within matrix GO, which is exfoliated and decorated (Vimuna, V. M., *et al.,* 2018). It can be seen that as result of interaction between filler and matrix within nanohybrids of MnO_2@CA and MnO_2@Tau, GO acts as spacer that prevents the aggregation of filler nanoparticles. Similarly, MnO_2@CA and MnO_2@Tau inhibit restacking of GO sheets. The above properties may be benefited to enhanced adsorption capacity (Liang, C., *et al.,* 2018).

Crinkled GO nanosheets were well exfoliated by surfaced-deposited functionalized MnO_2 particles. The flexible and ultrathin GO sheets wrapped the functionalized MnO_2 particles and imparted the ability for enhanced adsorption. It can be seen that in both types of hybrids, the filler MnO_2@CA and MnO_2@Tau are not aggregated and uniformly distributed. On the basis of the above analysis, it is reasonable to conclude that layer-by-layer composites were successfully prepared. The morphological changes such as porosity and surface heterogeneity induced through nanohybrid formation are expected to improve performance of these materials compared to neat and functionalized MnO_2 nanoparticles (Liang, C., *et al.,* 2018; Hu, H., *et al.,* 2022).

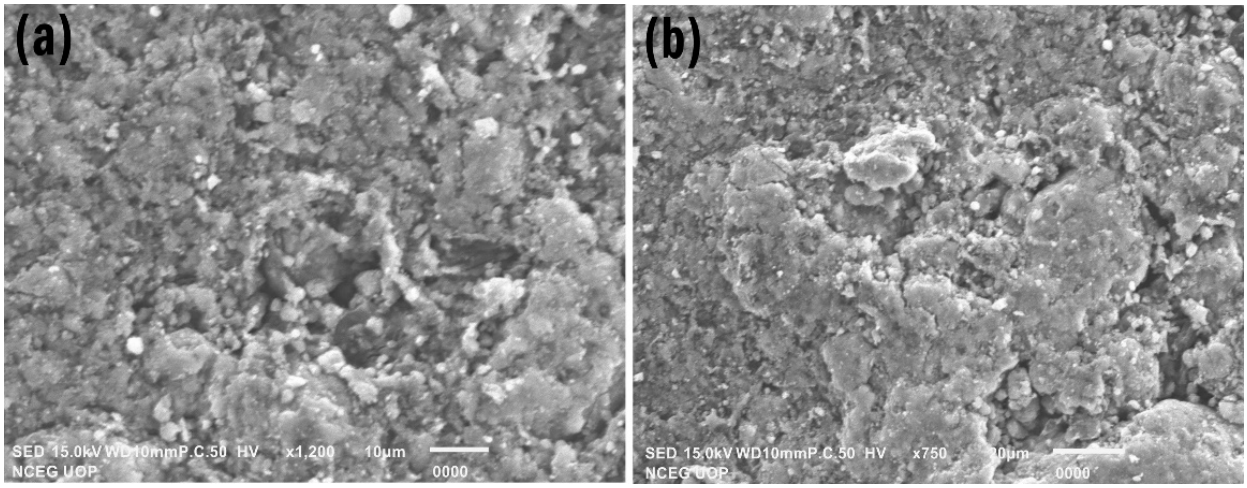

Fig. 5. SEM images of GO–MnO2@CA composite at different magnifications

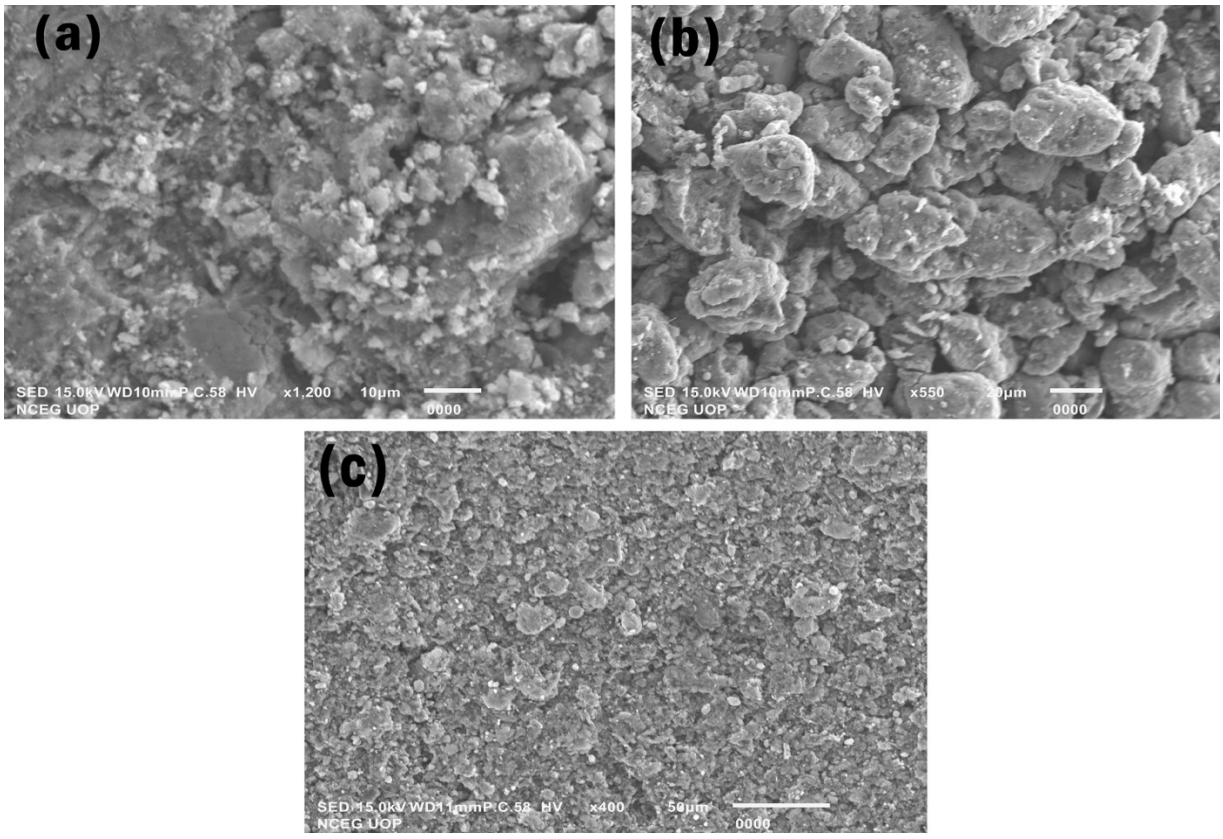

Fig. 6. SEM images of GO–MnO2@Tau nanohybrid at different magnifications

3.5 Thermal gravimetric analysis (TGA)

The TGA was performed to study thermal behavior of the synthesized GO-MnO_2@CA and GO-MnO_2@Tau as given in Figure 7. (a), (b). The thermal degradation of GO-MnO_2@CA occurred in two stages. In the first step GO-MnO_2@CA have shown 14% weight loss due to chemically adsorbed water molecules (<100Cº) [36]. The second step corresponds to 15% weight loss at around 190 ºC as a result of decomposition of functional group like hydroxyl, epoxy, carboxylic present on GO and also that of the carbon skeleton of graphene layers. The residue around 50% could be ascribed to the existence of functionalized MnO_2@CA in the nanohybrids.

TGA of the GO-MnO_2@Tau showed two step thermal degradation as unraveled by Figure 7. (a), (b). In GO-MnO_2@Tau, the weight loss from 100ºC to 130ºC is attributed to loss of adsorbed H_2O, which was followed by the decomposition of GO between 200°C to 250°C and the remaining 55% could be recognized as residue of MnO_2@Tau nanohybrid (Sathish, M., *et al.,* 2011). The degradation patterns of both nanohybrids are alike, showing the absence of an effect of functionalization by CA and TAU on thermal stability of these materials. The temperature-dependent behavior manifested by nanohybrids reveals the retention of thermal properties of GO (Farivar, F., *et al.,* 2021) .

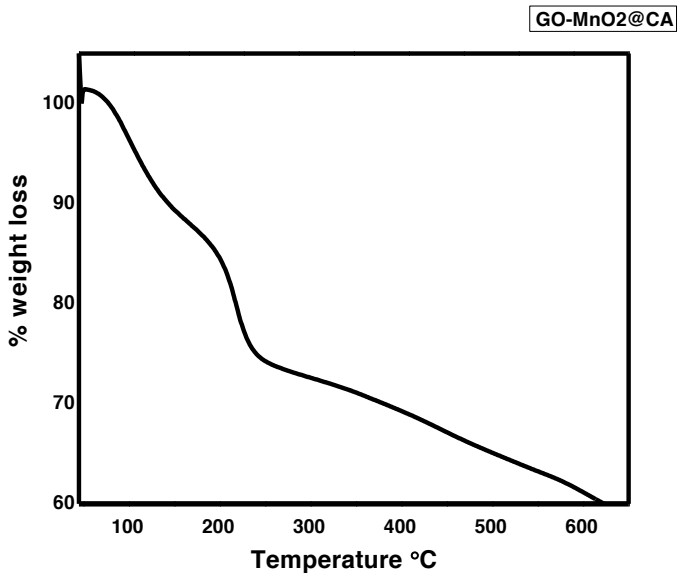

Fig. 7. (a). TGA of GO-MnO2@CA

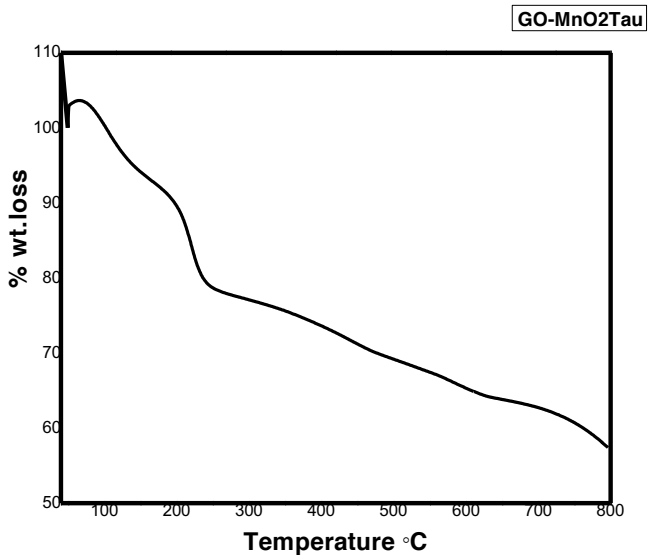

Fig. 7 (b). TGA of GO-MnO_2@CA

3.6 Adsorption study

The UV-Visible was performed to study the adsorption behavior of the GO-MnO_2@CA and GO-MnO_2@Tau by using MB dye at λ_{max} = 658 nm with different concentration in aqueous solution. The rate of adsorption of GO-MnO_2@CA and GO-MnO_2@Tau nanohybrids were monitored at different concentration and temperature.

3.7 The Effect of Concentration of Nanocomposite

In this work, three different concentrations (0.005g, 0.01g and 0.015g) of GO-MnO_2@CA and GO-MnO_2@Tau adsorbent were studied, while the other parameters remained constant It can be seen from the experimental results that by increasing the quantity of adsorbent, the adsorption increases Figure 8. & 9. This is expected due to availability of greater number of active sites for MB adsorption (Walton, I. M., *et al.,* 2016; Kumar, N., *et al.,* 2014). For GO-MnO_2@Tau, above 90% removal of MB was observed irrespective of the quantity of adsorbent used. On the other hands the removal achieved with GO-MnO_2@CA, was between 70-80%. This is probable as taurine is a bifunctional compound and possesses $–NH_3^+$as well as $–SO_3^-$ group in the zwitterion, hence it can more effectively interact with cationic methylene blue compared to caproic acid, which on utilization of carboxyl group in hybrid formation can only interact with the dye through van der Waal forces. Hence, most of the dye adsorption is occurring through entrapment in to pores of the adsorbent.

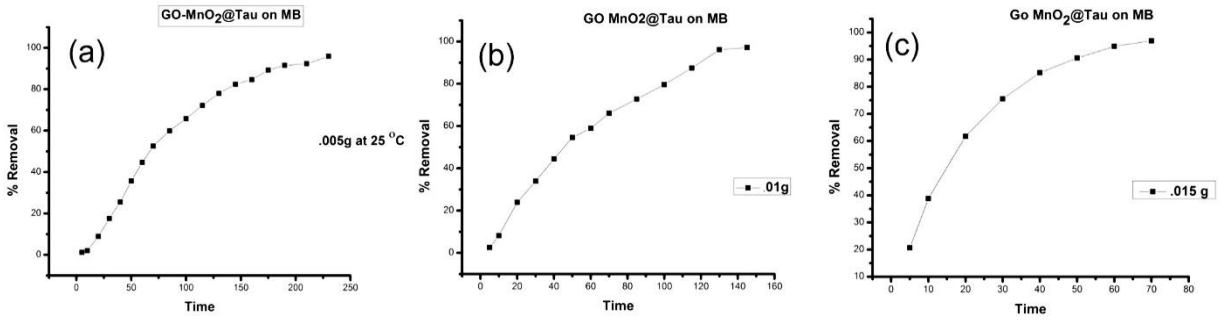

Fig. 8. Effect of different amount of GO-MnO2@Tau Nanocomposite on MB at .005, .01, and 0.015g.

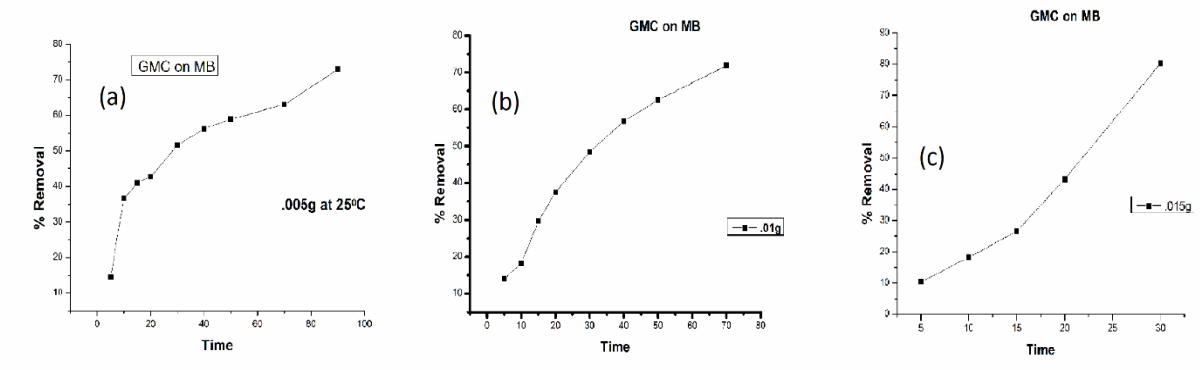

Fig. 9. Effect of various amount of GO-MnO2@CA Nanocomposite on MB at .005, .01, and 0.015g.

3.9 Temperature effect

Temperature affects the adsorption process in two ways. First, the diffusion rate is increased by increasing the temperature across the external boundary of adsorbate and in the inner pores of the adsorbent. As temperature increases, the average kinetic energy also increases, as a result, the diffusion rate increases and the solution viscosity decreases. Secondly, the adsorptions equilibrium of the adsorbent is affected by temperature. In present work, the adsorption process was studied at three different temperatures 25°C, 40°C and 55°C, with the constant amount of adsorbent 0.005 g (50mL) in solution. The % removal of MB is shown in Figure 8. & Figure 9. The results showed that with an increase in temperature, the adsorption capacity also increased. Normally this happens in chemisorption, where the increase in temperature activates the adsorbate molecules to obtain enough energy to interact with functionalities on the surface of the adsorbent.

3.10 Adsorption kinetics Model

To obtain the information about the rate constant and order of reaction, two important kinetics models, *pseudo* first order and *pseudo* second order were applied to obtain the experimental results for GO-MnO_2@Tau and GO-MnO_2@CA nanohybrids as initial concentration of 50 ml for MB.
Pseudo first order case assumes that the process of adsorption is directly affected by the free active sites present on adsorbent. For pseudo1st order kinetics model log (qe-qt) was plotted versus time (t) as given in Figure 10. (a), (b) respectively. The results in this case didn't fit the data, which indicated that this kinetic was not followed by the adsorption process
The *pseudo* second order model is related to the adsorption process of adsorbate molecules on adsorbent occurring at any time at equilibrium position. Figure 10 ©, (d) shows the plots t/qt versus time (t) for MB adsorption. Since, the coefficient of regression R^2 for *pseudo* second order model was close to 1, it was considered valid for adsorption taking place in our systems.

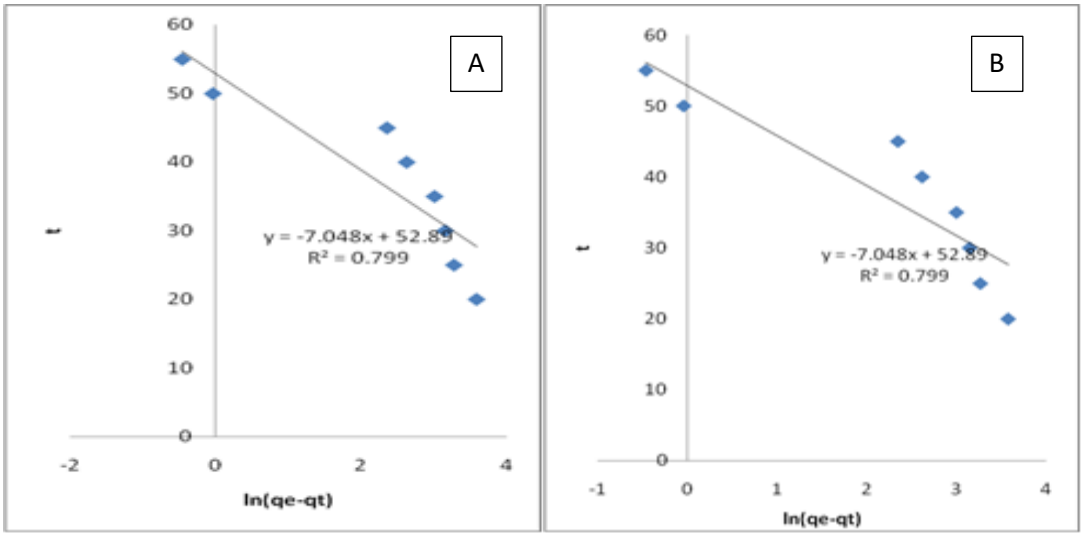

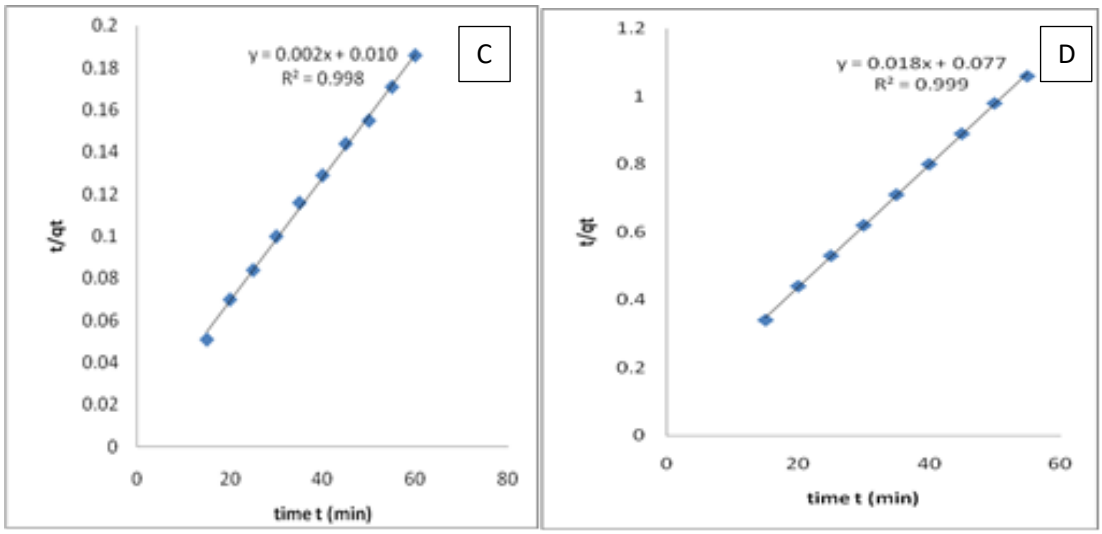

Fig. 10. (a) the pseudo 1st order kinetics of GO-MnO2@CA on MB, **(b)** represent the psedo 1st order reaction of GO-MnO2@Tau on MB, **(c)** represent the pseudo 2nd order reaction of GO-MnO2@CA on MB, **(d)** represent the pseudo 2nd order reaction of GO-MnO2@Tau on MB

3.11 Antibacterial activity

Two bacterial strains such as *S. aureus* (Gram +ive) and *E. coli* (Gram-ive) were chosen to study the antibacterial potential of nanohybrids of GO-MnO_2@CA and GO-MnO_2@Tau at three different concentrations i.e., 50µl, 75µl and 100µl. In each case, the zone of inhibition was measured using disk diffusion method. Antibacterial activity of GO-MnO_2@CA and GO-MnO_2@Tau against *E. coli* than the zone of inhibition is 10mm for 50µl of GMT and GMC is shown in Figure 11. Similarly, GMT and GMC nanohybrids also show a high zone of inhibition against *S. aureus.* Our results showed that increased concentration of GO-MnO_2@Tau and GO-MnO_2@CA nanocomposite has antagonist effects against these pathogens. This antibacterial activity can be ascribed to direct contact with pathogens owing to sheet like structure, presence of reactive oxygen species, bacterial membrane perforation (Du, T., *et al.,* 2020). Bacterial cell membranes comprise negatively charged lipids and cationic -NH_3^+ of taurine can bind to membrane surface though electrostatic interactions and the hydrocarbon chain of caproic acid can provide anchoring of nanohybrids through intercalation among lipid alkyl chains (Yeh, Y. C., *et al.,* 2020)**.** The light harnessing ability of nano structures also augments the antimicrobial performance (Warsi, M. F., *et al.,* 2022). Thus, it may have inferred that both nanohybrids are more effective inhibitors of *S. aureus* as compared to *E. coli* strains. Both nanohybrids had effectively destroyed selected pathogens in contaminated water and can play an important role in wastewater treatment.

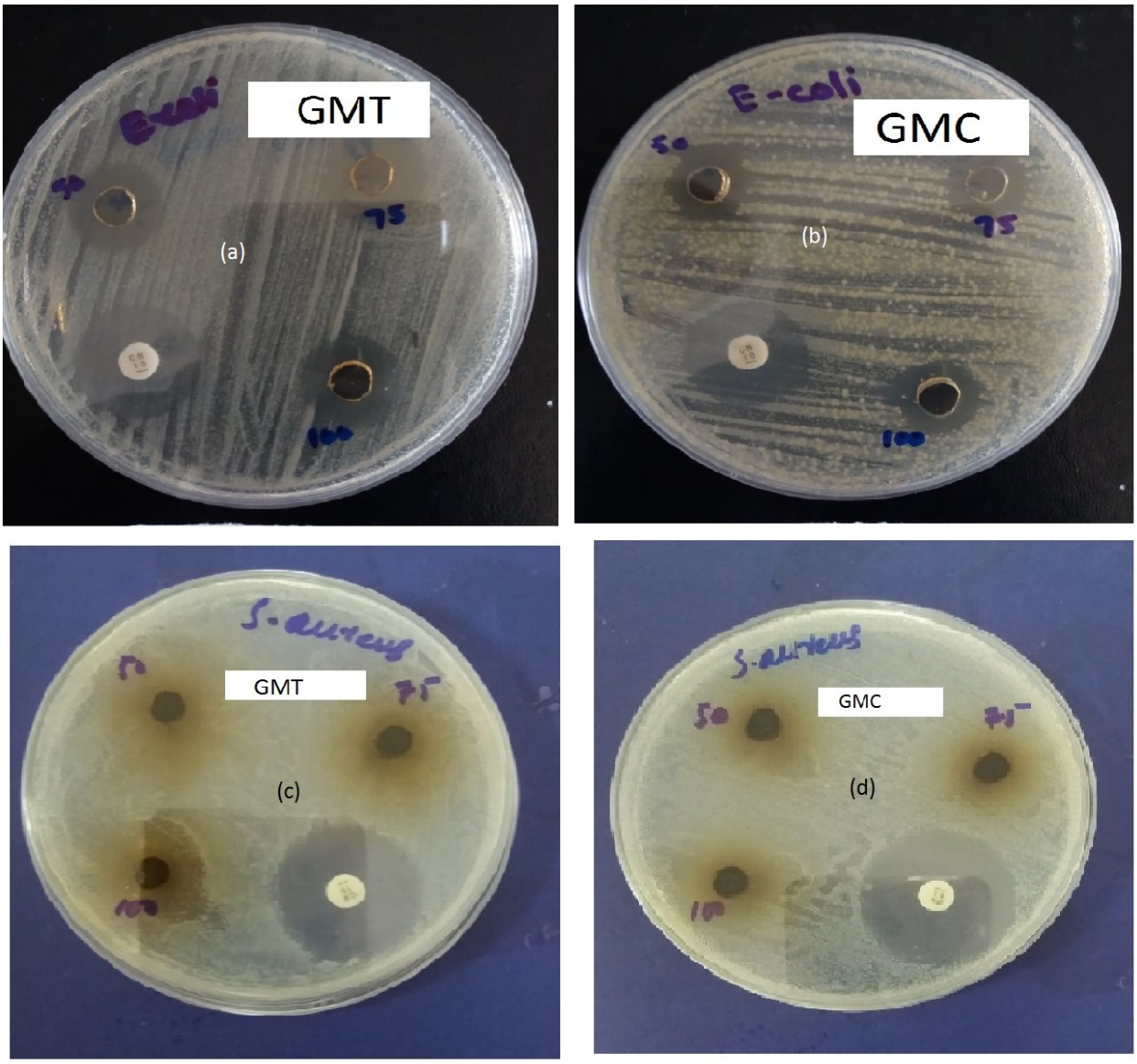

Fig. 11. Inhibitory zones of GO-MnO_2@CA and GO-MnO_2@Tau nanohybrids against (a) *S. aureus* (b) *Escherichia coli*

4. Conclusion

In the present study, nanohybrids GO–MnO_2@CA and GO-MnO_2@ Tau were successfully fabricated and characterized using FT-IR, SEM and XRD. During adsorption studies, both composites were found to be effective materials for adsorptive removal of industrial dyes such as MB. The adsorption was augmented by increase in quantity of adsorbent as well with temperature. The direct dependence of temperature reflected that chemisorption occurred in both the case. The validity experiments showed that the process followed *pseudo* second order kinetics. These nanohybrids were found to possess antibacterial activity against harmful pathogens like *E. coli* and *S. aureus*. Based on their adsorptive potential and antibacterial effects, they could be utilized effectively for treatment of waste water.

ACKNOWLEDGMENTS.
One of us M. H A. expresses thanks to Taif University researchers supporting Project TURSP2020/91, Taif Saudi Arabia.

References

Balasubramanian, N., Sakthivel, N., Prabhu, S., Ramesh, R., Kumar, S.A., Anbarasan, P.M. (2022) Design of Cube-like MnO2/r-GO Nanocomposite as a Superior Electrode Material for an Asymmetric Supercapacitor. J.Solid. State Sci. Technol, 11(7), 071010.

Baruah, U., & Chowdhury, D. (2018) Adv. Mater. Lett., 9 (7), 516–525.

Bera, M., Gupta, P., & Maji, P. K. (2018) Facile one-pot synthesis of graphene oxide by sonication assisted mechanochemical approach and its surface chemistry. Journal of nanoscience and nanotechnology, 18(2), 902-912.

Beshir, L., M. (2018) Determination of Cadmium, Chromium and Lead from Industrial Wastewater in Kombolcha Town, Ethiopia Using FAAS. J. Environ. Anal. Chem., 05(03).

Çiplak, Z., Yildiz, N., & Çalimli, A. (2015) Investigation of graphene/Ag nanocomposites synthesis parameters for two different synthesis methods. Fullerenes, Nanotubes and Carbon Nanostructures, 23(4), 361-370.

Du, T., Chen, S., Zhang, J., Li, T., Li, P., Liu, J., Du, X., Wang, S. (2020) Antibacterial Activity of Manganese Dioxide Nanosheets by ROS-Mediated Pathways and Destroying Membrane Integrity, Nanomaterials (Basel), 10(8), 1545.

Elemike, E. E., Dare, E. O., Samuel, I. D., & Onwuka, J. C. (2016) 2-Imino-(3, 4-dimethoxybenzyl) ethanesulfonic acid Schiff base anchored silver nanocomplex mediated by sugarcane juice and their antibacterial activities. Journal of applied research and technology, 14(1), 38-46.

Farivar, F., Yap, P. L., Hassan, K., Tung, T., Tran, D., Pollard, A., Losic, D.usan. (2021) Unlocking Thermogravimetric Analysis (TGA) in the Fight against “Fake Graphene” Materials. Carbon. 179, 505-513

Fei, J. B., Cui, Y., Yan, X. H., Qi, W., Yang, Y., Wang, K. W., & Li, J. B. (2008) Controlled preparation of MnO2 hierarchical hollow nanostructures and their application in water treatment. Advanced Materials, 20(3), 452-456.

Gund, G. S., Dubal, D. P., Chodankar, N. R., Cho, J. Y., Gomez-Romero, P., Park, C., & Lokhande, C. D. (2015) Sci. Re. 5(1).

Gupta, V. K., Fakhri, A., Agarwal, S., & Sadeghi, N. (2017) Synthesis of MnO2/cellulose fiber nanocomposites for rapid adsorption of insecticide compound and optimization by response surface methodology. International journal of biological macromolecules, 102, 840-846.

Hoseinpour, V., Souri, M., & Ghaemi, N. (2018) Green synthesis, characterisation, and photocatalytic activity of manganese dioxide nanoparticles. Micro & Nano Letters, 13(11), 1560-1563.

Hu, H., Wen, W., Ou, J. Z. (2022) Construction of adsorbents with graphene and its derivatives for wastewater treatment: a review, Environmental Science: Nano (advance article).

Hu, Z., Zu, L., Jiang, Y., Lian, H., Liu, Y., Li, Z., & Cui, X. (2015) High specific capacitance of polyaniline/mesoporous manganese dioxide composite using KI-H2SO4 electrolyte. Polymers, 7(10), 1939-1953.

Jayandran, M., Muhamed Haneefa, M., & Balasubramanian, V. (2015) Green synthesis and characterization of Manganese nanoparticles using natural plant extracts and its evaluation of antimicrobial activity. J App Pharm Sci, 5 (12), 105-110.

Kumar, N., Thomas, S., Tokas, R. B., & Kshirsagar, R. J. (2014) Investigation on the adsorption characteristics of sodium benzoate and taurine on gold nanoparticle film by ATR–FTIR spectroscopy. Spectrochimica Acta Part A: Molecular and Biomolecular Spectroscopy, 118, 614-618.

Kumar, R. R., Thanigaivel, S., Priya, A. K., Karthick, A., Malla, C., Jayaraman, P., Muhibbullah, M., Alshgari, R.A., Karami, A. M. (2022) Fabrication of MnO2 Nanocomposite on GO Functionalized with Advanced Electrode Material for Supercapacitors. Journal of Nanomaterials , 2022. https://doi.org/10.1155/2022/7929270.

Lei, Z., Shi, F., & Lu, L. (2012) Incorporation of MnO2-coated carbon nanotubes between graphene sheets as supercapacitor electrode. ACS applied materials & interfaces, 4(2), 1058-1064.

Liang, C., Feng, X., Yu, J., & Jiang, X. (2018) Facile one-step hydrothermal syntheses of graphene oxide–MnO 2 composite and their application in removing heavy metal ions. Micro & Nano Letters, 13(8), 1179-1184.

Ossonon, B. D., & Bélanger, D. (2017) Synthesis and characterization of sulfophenyl-functionalized reduced graphene oxide sheets. RSC advances, 7(44), 27224-27234.

Pattnaik, S., Swain, K., & Lin, Z. (2016) Graphene and graphene-based nanocomposites: biomedical applications and biosafety. Journal of Materials Chemistry B, 4(48), 7813-7831.

Paulchamy, B., Arthi, G., & Lignesh, B. D. (2015) A simple approach to stepwise synthesis of graphene oxide nanomaterial. J Nanomed Nanotechnol, 6(1), 1.

Qu, J., Shi, L., He, C., Gao, F., Li, B., Zhou, Q., & Qiu, J. (2014) Highly efficient synthesis of graphene/MnO2 hybrids and their application for ultrafast oxidative decomposition of methylene blue. Carbon, 66, 485-492.

Rafi, M., Samiey, B., & Cheng, C. H. (2018) Study of adsorption mechanism of congo red on graphene oxide/PAMAM nanocomposite. Materials, 11(4), 496.

Sathish, M., Mitani, S., Tomai, T., & Honma, I. (2011) MnO2 assisted oxidative polymerization of aniline on graphene sheets: Superior nanocomposite electrodes for electrochemical supercapacitors. Journal of Materials Chemistry, 21(40), 16216-16222.

Sharma, N., Sharma, V., Jain, Y., Kumari, M., Gupta, R., Sharma, S. K., & Sachdev, K. (2017) Synthesis and characterization of graphene oxide (GO) and reduced graphene oxide (rGO) for gas sensing application. In Macromolecular Symposia (Vol. 376, No. 1, p. 1700006).

Singu, B. S., & Yoon, K. R. (2017) Synthesis and characterization of MnO2-decorated graphene for supercapacitors. Electrochimica Acta, 231, 749-758.

Singu, B. S., & Yoon, K. R. (2017) Synthesis and characterization of MnO2-decorated graphene for supercapacitors. Electrochimica Acta, 231, 749-758.

Stobinski, L., Lesiak, B., Malolepszy, A., Mazurkiewicz, M., Mierzwa, B., Zemek, J., & Bieloshapka, I. (2014) Graphene oxide and reduced graphene oxide studied by the XRD, TEM and electron spectroscopy methods. Journal of Electron Spectroscopy and Related Phenomena, 195, 145-154.

Vimuna, V. M., Athira, A. R., & Xavier, T. S. (2018) AIP, Conference proceedings, 030136.

Walton, I. M., Cox, J. M., Benson, C. A., Patel, D. D. G., Chen, Y. S., & Benedict, J. B. (2016) The role of atropisomers on the photo-reactivity and fatigue of diarylethene-based metal–organic frameworks. New Journal of Chemistry, 40(1), 101-106.

Walton, I. M., Cox, J. M., Benson, C. A., Patel, D. D. G., Chen, Y. S., & Benedict, J. B. (2016) The role of atropisomers on the photo-reactivity and fatigue of diarylethene-based metal–organic frameworks. New Journal of Chemistry, 40(1), 101-106.

Wang, H., Fu, Q., & Pan, C. (2019) Green mass synthesis of graphene oxide and its MnO2 composite for high performance supercapacitor. Electrochimica Acta, 312, 11-21.

Wang, J. W., Chen, Y., & Chen, B. Z. (2015) A synthesis method of MnO2/activated carbon composite for electrochemical supercapacitors. Journal of the Electrochemical Society, 162(8), A1654.

Wang, N., Li, X., Yang, J., Shen, Y., Qu, J., Hong, S., & Yu, Z. Z. (2016) Fabrication of a compressible PU@ RGO@ MnO 2 hybrid sponge for efficient removal of methylene blue with an excellent recyclability. Rsc Advances, 6(91), 88897-88903.

Warsi, M. F., Chaudhary, K., Zulfiqar, S., Ibrahim, A. R., Safari, A. A., Zeeshan, H. M., Philips, O. A., Shahid, M., Suleman, M. (2022) Copper and silver substituted MnO2 nanostructures with superior photocatalytic and antimicrobial activity. Ceramics International, 48 (4), 4930-4939.

Wei, C., Xu, C., Li, B., Du, H., & Kang, F. (2012) Preparation and characterization of manganese dioxides with nano-sized tunnel structures for zinc ion storage. Journal of Physics and Chemistry of Solids, 73(12), 1487-1491.

Wu, H., Tang, B., & Wu, P. (2014) Development of novel SiO2–GO nanohybrid/polysulfone membrane with enhanced performance. Journal of Membrane Science, 451, 94-102.

Yang, W., Zhang, J., Ma, Q., Zhao, Y., Liu, Y., He, & He, H. (2017) Sci. Rep., 7(1).

Yeh, Y. C., Huang, T. H., Yang, S. C., Chen, C. C., Fang, J. Y. (2020) Nano-Based Drug Delivery or Targeting to Eradicate Bacteria for Infection Mitigation: A Review of Recent Advances. Frontiers in Chemistry, 24 (8) 286.

Yu, T., Sun, Y., Zhe, C., Wang, W., & Rao, P. (2017) J., Mater. Sci. Chem. Eng. 05 (10) 12–25.

Zhang, Y., Zhang, J., Huang, X., Zhou, X., Wu, H., & Guo, S. (2012) Assembly of graphene oxide–enzyme conjugates through hydrophobic interaction. Small, 8(1), 154-159.

Submitted: 07/04/2022
Revised: 29/08/2022
Accepted: 11/09/2022
DOI: 10.48129/kjs.19959